J. Fluid Mech. (1993), *vol.* 248, *pp.* 583–604

Convection in a rotating cylinder. Part 1 Linear theory for moderate Prandtl numbers

By H. F. GOLDSTEIN,[1] E. KNOBLOCH,[1] I. MERCADER[2] AND M. NET[2]

[1] Department of Physics, University of California, Berkeley, CA 94720, USA

[2] Departament de Física Aplicada, Universitat Politècnica de Catalunya, E 08034 Barcelona, Spain

(Received 13 April 1992)

The onset of convection in a uniformly rotating vertical cylinder of height h and radius d heated from below is studied. For non-zero azimuthal wavenumber the instability is a Hopf bifurcation regardless of the Prandtl number of the fluid, and leads to precessing spiral patterns. The patterns typically precess counter to the rotation direction. Two types of modes are distinguished: the fast modes with relatively high precession velocity whose amplitude peaks near the sidewall, and the slow modes whose amplitude peaks near the centre. For aspect ratios $\Gamma \equiv d/h$ of order one or less the fast modes always set in first as the Rayleigh number increases; for larger aspect ratios the slow modes are preferred provided that the rotation rate is sufficiently slow. The precession velocity of the slow modes vanishes as $\Gamma \to \infty$. Thus it is these modes which provide the connection between the results for a finite-aspect-ratio system and the unbounded layer in which the instability is a steady-state one, except in low Prandtl number fluids.

The linear stability problem is solved for several different sets of boundary conditions, and the results compared with recent experiments. Results are presented for Prandtl numbers σ in the range $6.7 \leqslant \sigma \leqslant 7.0$ as a function of both the rotation rate and the aspect ratio. The results for rigid walls, thermally conducting top and bottom and an insulating sidewall agree well with the measured critical Rayleigh numbers and precession frequencies for water in a $\Gamma = 1$ cylinder. A conducting sidewall raises the critical Rayleigh number, while free-slip boundary conditions lower it. The difference between the critical Rayleigh numbers with no-slip and free-slip boundaries becomes small for dimensionless rotation rates $\Omega h^2/\nu \geqslant 200$, where ν is the kinematic viscosity.

1. Introduction and background

Rayleigh–Bénard convection in a pure fluid has been studied in the past as a particularly simple system exhibiting spontaneous pattern formation when the Rayleigh number R exceeds a critical value (hereafter referred to as R_c). Substantial progress has been made in understanding the process of pattern selection at small amplitudes, i.e. for $|R - R_c| \ll R_c$. Most theoretical treatments (see e.g. Chandrasekhar 1961) assume that the system is unbounded in the horizontal plane. This assumption facilitates the solution of the linear stability problem and hence the location of R_c. In a non-rotating system it is known that the resulting instability is a steady-state one, and leads to a pattern either of rolls or of hexagons. Rolls are found when the boundary conditions at top and bottom are identical and non-Boussinesq effects are

absent. If either of these requirements is not fulfilled the initial transition is hysteretic and gives rise to hexagons (Schlüter, Lortz & Busse 1965; Busse 1978). The primary difference between these two cases is the absence of a reflection symmetry in the midplane of the layer in the latter case. The plane layer has another important reflection symmetry as well. This is a reflection in any vertical plane. When this symmetry is broken, e.g. by rotating the layer about the vertical, the initial instability may set in as overstability. Chandrasekhar (1961) shows that in an unbounded layer this occurs only for Prandtl numbers $\sigma < 0.68$; for water ($\sigma = 6.7$) the instability continues to be a steady-state instability. The broken reflection symmetry in vertical planes has, however, a profound effect on the stability of the resulting rolls. As the rotation rate increases, the initial rolls lose stability to rolls oriented at approximately 59° with respect to the initial pattern in the direction of rotation, and these are in turn unstable to a roll pattern at another 59° relative to them, and so on (Küppers & Lortz 1969). Thus for large enough rotation rates no stable rolls are present near onset, even in systems with a midplane reflection symmetry. The situation becomes quite different when the translation invariance of the plane layer is broken as well, e.g. by considering convection in a finite container. To preserve rotational invariance we consider here convection in cylindrical containers. In the non-rotating case the onset of convection continues to be a steady-state one, although the pattern that forms near onset may take a form quite different from the roll pattern characteristic of the unbounded system. This pattern, first described by Jones & Moore (1979) and by Buell & Catton (1983*a*; see also Marqués *et al.* 1992), is a reflection-symmetric spoke-like pattern with a non-zero azimuthal wavenumber m. Recent experiments on convection in water revealed, however, that in a rotating cylinder the corresponding pattern is no longer reflection symmetric (in fact it is an m-fold spiral) and that it precesses in the rotating frame (Zhong, Ecke & Steinberg 1991; Ecke, Zhong & Knobloch 1992). In this paper these observations are supported by a detailed solution of the linear stability problem for the conduction solution in a uniformly rotating right circular cylinder heated from below. We find that the patterns do indeed precess and that there are in fact two families of such precessing patterns. The latter is in distinct contrast to the non-rotating problem in which only one type of unstable mode is present. We discuss the origin and properties of these unstable modes and determine the conditions under which one or other type of unstable mode is preferred.

It was pointed out by Goldstein & Knobloch (1991) and Ecke *et al.* (1992) that the observation of precessing patterns implies that the onset of convection is now a Hopf bifurcation, even though the fluid is water, and that in a rotating system a Hopf bifurcation is in fact to be expected whenever the azimuthal wavenumber m is non-zero. The argument goes as follows. Consider, say, the temperature perturbation Θ from the conduction state. In a cylindrical container, it follows that

$$\Theta(r,\phi,z,t) = \mathrm{Re}\{a(t)\,\mathrm{e}^{\mathrm{i}m\phi} f_m(r,z)\} + \ldots, \tag{1}$$

where (r,ϕ,z) are cylindrical coordinates, $f_m(r,z)$ is the eigenfunction of the mode m and $a(t)$ is its complex amplitude. Here, the omitted terms (...) involve spatial harmonics of the fundamental generated by nonlinear terms; these modes are 'slaved' to the evolution of a. We assume that $m \neq 0$ so that the instability breaks azimuthal symmetry. When the cylinder is non-rotating and the boundary conditions are homogeneous in ϕ the equation satisfied by a must commute with the following symmetries:

$$\text{rotations} \quad \phi \to \phi + \theta: \quad a \to a\,\mathrm{e}^{\mathrm{i}m\theta}, \tag{2}$$

$$\text{reflections} \quad \phi \to -\phi: \quad a \to \bar{a}. \tag{3}$$

It follows that for $\epsilon \equiv (R-R_c)/R_c \ll 1$ the amplitude a satisfies an equation of the form

$$\dot{a} = g(|a|^2, \epsilon)\, a, \tag{4}$$

where the function g is forced by (3) to be real. Since a is small, we may expand g in a Taylor series,

$$\dot{a} = \epsilon a + \alpha |a|^2 a + \ldots, \tag{5}$$

obtaining

$$\dot{A} = \epsilon A + \alpha A^3 + \ldots, \quad \dot{\Phi} = 0, \tag{6}$$

where $a = A\, e^{i\Phi}$ and A and Φ are real. The equation $\dot{\Phi} = 0$ is a consequence of the reflection symmetry of the pattern. When the cylinder is rotated about the vertical with angular velocity Ω the reflection symmetry (3) is broken. Consequently the function g acquires an imaginary part, and (5) becomes

$$\dot{a} = (\epsilon + i\Omega\delta)\, a + (\alpha + i\Omega\beta)\, |a|^2 a + \ldots, \tag{7}$$

where now ϵ, δ, α, and β are all functions of Ω^2. In terms of the real variables A, Φ we now have

$$\dot{A} = \epsilon A + \alpha A^3 + \ldots, \quad \dot{\Phi} = \Omega(\delta + \beta A^2 + \ldots). \tag{8}$$

Consequently the broken reflection symmetry turns the steady-state bifurcation in the non-rotating system into a Hopf bifurcation in the rotating system. Moreover, since $\dot{\Phi}$ is the rate of change of the azimuthal phase, it is to be identified with the precession frequency ω_p in the rotating frame. In particular, Θ takes the form

$$\Theta = \mathrm{Re}\{A\, e^{i(m\phi + \omega_p t)} f_m(r, z)\} + \ldots. \tag{9}$$

The bifurcation is thus to a *rotating wave* (Chossat 1982; Rand 1982). Equation (8) shows that the precession frequency of a steady-state pattern is given by

$$\omega_p = \Omega\left(\delta - \frac{\beta}{\alpha}\epsilon\right) + O(\epsilon^2). \tag{10}$$

We denote the precession frequency at onset ($\epsilon = 0$) by $\omega_c (\equiv \Omega\delta)$. The dependence of ω_p on Ω and ϵ suggested by the above theory has been verified experimentally (Ecke *et al.* 1992), and the experimental fits were used to determine the values of δ and β/α in the limit $\Omega \to 0$. These observations motivate a re-examination of the linear stability problem for a rotating cylinder in order to seek quantitative agreement between the above theory and the experimental data.

The linear stability problem in a rotating cylinder has been considered before by Buell & Catton (1983*b*). These authors, influenced by Chandrasekhar, assumed that for σ of order one the initial instability will be a steady one, and forced the growth rate to be real. They failed to notice that such a solution could not converge, presumably because, as shown below, the precession frequency ω_c is rather small. In the present paper we solve the linear stability problem by two different methods and for two different sets of boundary conditions at top and bottom. We calculate R_c and ω_c as a function of both the rotation rate and of the cylinder aspect ratio, and compare the results with existing experiments. We do not consider the nonlinear problem. We do, however, address the relation between the large-aspect-ratio linear stability results and those for moderate aspect ratios appropriate to the experiments. The remainder of the paper is organized as follows. In §2 we introduce the equations

and discuss the boundary conditions. In §3 we describe the two methods of solution we use. The results are presented in §4 and related to the experiments in §5.

2. The equations

We consider Boussinesq convection in a right cylinder of radius d and height h, filled with a pure fluid and rotating with constant and uniform angular velocity Ω about the vertical axis. We denote by Γ its aspect ratio d/h. The linearized, non-dimensionalized equations of motion take the form (Chandrasekhar 1961)

$$\left(\frac{1}{\sigma}\partial_t - \nabla^2\right)\boldsymbol{u} = -\nabla p + R\Theta\hat{\boldsymbol{z}} + \mathcal{T}\,\boldsymbol{u}\times\hat{\boldsymbol{z}}, \tag{11}$$

$$(\partial_t - \nabla^2)\,\Theta = w, \tag{12}$$

$$\nabla\cdot\boldsymbol{u} = 0, \tag{13}$$

where $\boldsymbol{u} = u\hat{\boldsymbol{r}} + v\hat{\boldsymbol{\phi}} + w\hat{\boldsymbol{z}}$ is the velocity field, Θ and p are the departures of the temperature and pressure from their conduction profiles, and $\hat{\boldsymbol{z}}$ is the unit vector in the vertical direction. The quantities $\mathcal{T} \equiv 2\Omega h^2/\nu$, $R \equiv g\alpha\Delta T h^3/\kappa\nu$, and $\sigma \equiv \nu/\kappa$ denote, respectively, the square root of the Taylor number, the Rayleigh number, and the Prandtl number. In these equations, length is in units of the layer thickness, h, and time is in units of the vertical thermal diffusion time, h^2/κ. Note that in writing (11) we have assumed that the centrifugal acceleration is sufficiently small that the effective gravity remains vertical. This assumption is justified for the rotation rates used by Zhong *et al.* (1991) for which $d\Omega^2/g < 0.01$ ($\mathcal{T} < 8548$).

We use two types of boundary conditions. Type A,

$$\partial_z u = \partial_z v = w = \Theta = 0 \quad \text{on} \quad z = 0, 1, \tag{14}$$

$$u = v = w = \partial_r \Theta = 0 \quad \text{on} \quad r = \Gamma, \tag{15}$$

correspond to free-slip, impenetrable, infinitely conducting horizontal plates at top and bottom, and a rigid, impenetrable, insulating sidewall. These boundary conditions are mathematically convenient in that they allow separation of variables in the vertical and azimuthal directions. Consequently an essentially exact solution of the eigenvalue problem is possible (see below). From an experimental point of view the free-slip boundary conditions at top and bottom are unrealistic. We therefore also solve (11)–(13) with the boundary conditions B:

$$u = v = w = \Theta = 0 \quad \text{on} \quad z = 0, 1, \tag{16}$$

$$u = v = w = \partial_r \Theta = 0 \quad \text{on} \quad r = \Gamma. \tag{17}$$

These boundary conditions correspond to rigid (i.e. no-slip) boundaries everywhere. The temperature boundary conditions on the sidewall are not critical to either method as long as they are independent of ϕ. We choose an insulating sidewall since this approximates best the experimental conditions (see §5).

The conduction solution, $u = v = w = \Theta = 0$, is stable to small perturbations below some critical value of the Rayleigh number, R_c, which depends, in general, on the aspect ratio, the Taylor number, and the Prandtl number, as well as on the boundary conditions. In other words, if we write the time dependence of a solution to the linear problem as e^{st}, then $\mathrm{Re}\,(s) < 0$ for all solutions when $R < R_c$. At $R = R_c$ there is for the first time a neutrally stable solution to the linear problem, i.e. $\mathrm{Re}\,(s) = 0$. If $\mathrm{Im}\,(s) = 0$, the bifurcation is steady state, and if $\mathrm{Im}\,(s) = \omega_c \neq 0$, we have a Hopf bifurcation with Hopf frequency ω_c.

3. Method of solution

In this section we provide a brief description of both methods that we use to solve the problem (11)–(13) with boundary conditions A or B. The first method (cf. Jones & Moore 1979) constructs exact solutions of the problem (11)–(13), (14)–(15) but is not available for the boundary conditions (16)–(17).

3.1. *Exact solution*

Equations (11)–(13) can be combined into a single equation for Θ,

$$\left[\left(\frac{1}{\sigma}\partial_t-\nabla^2\right)^2(\partial_t-\nabla^2)\nabla^2-R\nabla_{\mathrm{h}}^2\left(\frac{1}{\sigma}\partial_t-\nabla^2\right)+\mathscr{T}^2\partial_z^2(\partial_t-\nabla^2)\right]\Theta=0, \tag{18}$$

where ∇_{h}^2 is the two-dimensional Laplacian in the horizontal coordinates. In view of the boundary conditions (14)–(15), equation (18) has solutions of the form (cf. (1))

$$\Theta_{km}(r,\phi,z;k)=\mathrm{Re}\{J_m(kr)\,\mathrm{e}^{\mathrm{i}(m\phi+\omega t)}\}\sin(\pi z), \tag{19}$$

where m is a non-zero integer and $k=k(R,\omega,\mathscr{T},\sigma)$ is a solution to the dispersion relation,

$$\left(\frac{\mathrm{i}\omega}{\sigma}+k^2+\pi^2\right)^2(\mathrm{i}\omega+k^2+\pi^2)(k^2+\pi^2)-Rk^2\left(\frac{\mathrm{i}\omega}{\sigma}+k^2+\pi^2\right)+\mathscr{T}^2\pi^2(\mathrm{i}\omega+k^2+\pi^2)=0, \tag{20}$$

obtained by substituting (19) into (18). The solution (19) satisfies the boundary conditions at the top and bottom of the layer but not on the sidewall. In order to satisfy the boundary conditions on the sidewall, we note that (20) is quartic in k^2, and so has eight solutions $\pm k_j$, $j=1,2,3,4$. We can therefore write Θ_m as the linear combination

$$\Theta_m=\sum_{j=1}^{4}A_j J_m(k_j r)\,\mathrm{e}^{\mathrm{i}(m\phi+\omega t)}\sin(\pi z), \tag{21}$$

where the A_j are complex amplitudes to be determined by the boundary conditions. It is understood here and in what follow that the physical quantities are the real parts of the given solutions. Note that we need not explicitly use the solutions corresponding to the $-k_j$, since $J_m(-z)=(-1)^m J_m(z)$, and those solutions are therefore not linearly independent.

The corresponding velocity field may now be derived from (21) and the system (11)–(13). It is

$$w_m=\sum_{j=1}^{4}A_j\alpha_j J_m(k_j r)\,\mathrm{e}^{\mathrm{i}(m\phi+\omega t)}\sin(\pi z), \tag{22}$$

$$u_m=\pi\sum_{j=1}^{4}A_j\gamma_j\left(\beta_j\partial_r+\mathscr{T}\frac{\mathrm{i}m}{r}\right)J_m(k_j r)\,\mathrm{e}^{\mathrm{i}(m\phi+\omega t)}\cos(\pi z), \tag{23}$$

$$v_m=\pi\sum_{j=1}^{4}A_j\gamma_j\left(-\mathscr{T}\partial_r+\beta_j\frac{\mathrm{i}m}{r}\right)J_m(k_j r)\,\mathrm{e}^{\mathrm{i}(m\phi+\omega t)}\cos(\pi z), \tag{24}$$

where
$$\alpha_j\equiv\mathrm{i}\omega+k_j^2+\pi^2,\quad \beta_j\equiv\frac{\mathrm{i}\omega}{\sigma}+k_j^2+\pi^2,\quad\text{and}\quad \gamma_j=\frac{\alpha_j}{k_j^2\beta_j}. \tag{25}$$

We now impose the boundary conditions (15) at the sidewall, $r = \Gamma$, to obtain a set of linear, homogeneous equations for the A_j of the form

$$\boldsymbol{M}(R, \omega, \mathscr{T}, \sigma, m, \Gamma) \begin{pmatrix} A_1 \\ A_2 \\ A_3 \\ A_4 \end{pmatrix} = 0, \tag{26}$$

where $\boldsymbol{M}$ is a 4×4 complex-valued matrix which depends on the parameters both explicitly and implicitly through the k_j. The system (26) has a non-trivial solution for the A_j if and only if $\det(\boldsymbol{M}) = 0$. Since $\boldsymbol{M}$ is complex-valued, we must make the real and imaginary parts of the determinant vanish simultaneously. To find the non-trivial solutions to the linear problem with the required boundary conditions, we therefore hold the four parameters $\mathscr{T}$, σ, m, and Γ fixed and solve the system

$$\mathrm{Re}\,(\det(\boldsymbol{M}(R, \omega; \mathscr{T}, \sigma, m, \Gamma))) = 0, \tag{27}$$

$$\mathrm{Im}\,(\det(\boldsymbol{M}(R, \omega; \mathscr{T}, \sigma, m, \Gamma))) = 0 \tag{28}$$

numerically for $R = R_c^{(m)}$ and $\omega = \omega_c^{(m)}$. The values of $R_c^{(m)}$ can then be minimized over m to determine the wavenumber of the mode that sets in first; the corresponding Rayleigh number and precession frequency will be denoted by R_c and ω_c, respectively. We emphasize that while (27), (28) cannot be solved analytically, the implicit solutions solve the linear boundary-value problem exactly.

3.2. *Method based on velocity potentials*

Velocity potentials have proved extremely useful in a variety of problems in incompressible hydrodynamics. Their main purpose is to guarantee automatically the solenoidal nature of the velocity field. Moreover, depending on the geometry of the system, it is often possible to write the velocity field in terms of two scalar potentials which remain uncoupled at the boundaries. In the present problem any non-axisymmetric velocity field can be written in the form

$$\boldsymbol{u} = \boldsymbol{\nabla} \times (\chi \hat{\boldsymbol{r}} + \psi \hat{\boldsymbol{z}}), \tag{29}$$

where χ and ψ are the scalar potentials. The existence of both these potentials is guaranteed by the geometry and the no-slip boundary conditions on the sidewall (cf. Marqués 1990). In this case (11)–(13) are equivalent to

$$\left(\frac{1}{\sigma}\partial_t - \tilde{\nabla}^2\right)\omega_r = \frac{2}{r}\partial_z \omega_z + \frac{1}{r} R\, \partial_\phi \Theta + \mathscr{T}\, \partial_z u, \tag{30}$$

$$\left(\frac{1}{\sigma}\partial_t - \nabla^2\right)\omega_z = \mathscr{T}\, \partial_z w, \tag{31}$$

$$(\partial_t - \nabla^2)\,\Theta = w, \tag{32}$$

where $\boldsymbol{\omega} \equiv (\omega_r, \omega_\phi, \omega_z)$ is the vorticity, $\tilde{\nabla}^2 \equiv \nabla^2 + 2r^{-1}\partial_r + r^{-2}$, and

$$u = \frac{1}{r}\partial_\phi \psi, \quad w = -\frac{1}{r}\partial_\phi \chi, \tag{33}$$

$$\omega_r = -\left(\frac{1}{r^2}\partial^2_{\phi\phi} + \partial^2_{zz}\right)\chi + \partial^2_{rz}\psi, \tag{34}$$

$$\omega_z = -\nabla^2_{\mathrm{h}}\psi + \left(\frac{1}{r} + \partial_r\right)\partial_z \chi. \tag{35}$$

Boundary conditions (14)–(15) and (16)–(17) become

$$\psi = \partial_r \psi = \chi = \partial_r \Theta = 0 \quad \text{on} \quad r = \Gamma \tag{36}$$

together with

$$\left.\begin{array}{ll} \chi = \partial_{zz}^2 \chi = \partial_z \psi = \Theta = 0 & \text{(A)} \\ \chi = \partial_z \chi = \psi = \Theta = 0 & \text{(B)} \end{array}\right\} \quad \text{on} \quad z = 0, 1. \tag{37}$$

In the axisymmetric case a significant reduction in the order of the resulting equations is possible. For more details see Mercader, Net & Falques (1991). The above formulation becomes particularly useful for the nonlinear problem since it yields equations for two scalar functions only.

Equations (30)–(37) are solved by expanding the fields ψ, χ, and Θ in a Fourier series:

$$\chi(r, \phi, z, t) = \mathrm{i}\, \mathrm{e}^{st} \sum_m \chi_m(r, z)\, \mathrm{e}^{\mathrm{i}m\phi}, \tag{38}$$

$$\psi(r, \phi, z, t) = \mathrm{i}\, \mathrm{e}^{st} \sum_m \psi_m(r, z)\, \mathrm{e}^{\mathrm{i}m\phi}, \tag{39}$$

$$\Theta(r, \phi, z, t) = \mathrm{e}^{st} \sum_m \Theta_m(r, z)\, \mathrm{e}^{\mathrm{i}m\phi}, \tag{40}$$

yielding a set of coupled equations for $(\psi_m, \chi_m, \Theta_m)$ for each m. To solve these for the eigenvalue s given R, it is necessary to impose regularity conditions at $r = 0$, the central axis of the cylinder. The following boundary conditions suffice at $r = 0$:

$$\chi = \psi = \omega_r = \omega_z = 0; \tag{41}$$

if $m = 1$ the last but one condition is replaced by $\partial_r \omega_r = 0$.

For stress-free boundaries at top and bottom we expand the vertical structure of the eigenfunctions in a Fourier series. If $\Theta = 0$ at $z = 0, 1$ this series collapses to just a single term (see (19)). For rigid boundary conditions the vertical structure is expanded in Chebyshev polynomials. In both cases we have used Chebyshev polynomials for the radial dependence. The resulting problem is solved by a modified collocation method using the numerical techniques discussed in Marqués *et al.* (1992).

The procedure has been used to determine the onset of convection in a non-rotating cylinder for both sets of boundary conditions, and the results compared with existing ones obtained by other methods (Catton & Edwards 1970; Joseph 1971, for boundary conditions A, and Buell & Catton 1983*a*; Sabry 1984, for boundary conditions B). In addition, the results were confirmed using a different choice of the velocity potentials (Marqués *et al.* 1992); however, the formulation (29) was found to improve the accuracy for a given number of modes and was therefore adopted as the formulation of choice. The results presented below were typically obtained with 18 collocation points in the vertical and 16 in the horizontal. For boundary conditions B, the resulting errors are estimated to be 1.25% in R_c and 0.5% in ω_c for $\Gamma = 1$, $\Omega = 2.5 \times 10^3$, increasing to 1.5% in R_c and 2% in ω_c for $\Gamma = 2.5$, $\Omega = 10^3$. Here and hereafter the symbol Ω is used to denote the *dimensionless* rotation rate $\frac{1}{2}\mathscr{T}$. For boundary conditions A the accuracy of the procedure can be checked against the exact results. The details of this comparison are presented in table 1. The agreement is excellent ($\ll 1\%$) in all the cases considered.

4. Results

In this section, we describe our results for the two sets of boundary conditions. The results for case A were obtained using the procedure described in §3.1 and are essentially exact; those for boundary conditions B were obtained using the technique

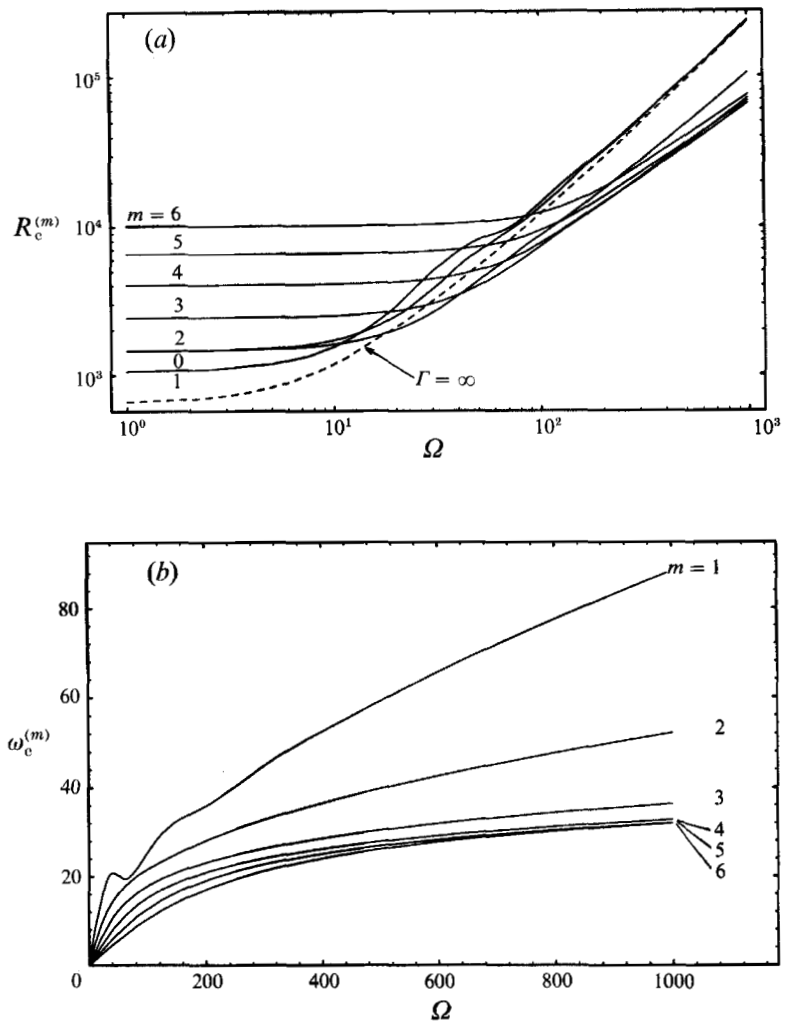

FIGURE 1. The linear stability results for the fast modes in a $\Gamma = 1$ cylinder with boundary conditions A and $\sigma = 7.0$. (*a*) The critical Rayleigh number $R_c^{(m)}$ and (*b*) the onset precession frequency $\omega_c^{(m)}$ as functions of the rotation rate Ω for several different values of the azimuthal wavenumber m. The dashed line in (*a*) indicates the corresponding result for an unbounded plane layer (Chandrasekhar 1961).

		Exact		Collocation	
Ω	m	R_c	ω_c	R_c	ω_c
10	1	1535.87	7.96	1535.87	7.96
20	2	1990.26	8.68	1990.24	8.68
50	3	3945.30	12.22	3945.30	12.22
250	4	17620.48	22.69	17620.48	22.69

TABLE 1. Comparison of critical Rayleigh number and Hopf frequency obtained by exact and collocation methods for boundary conditions A, with $\Gamma = 1.0$ and $\sigma = 6.7$

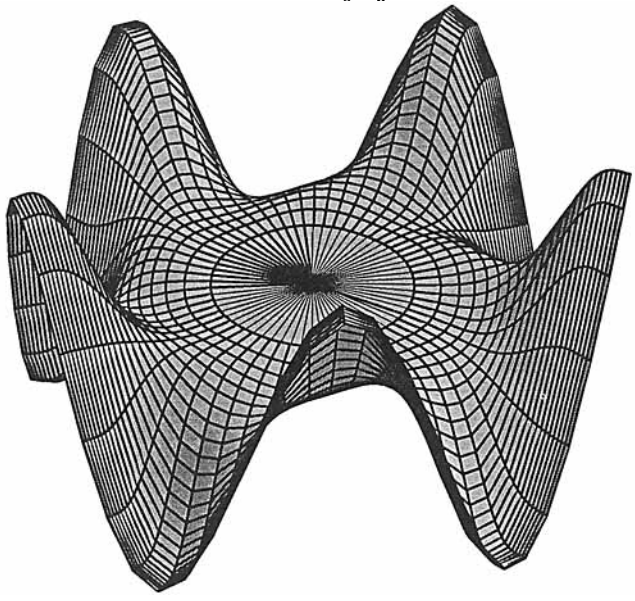

FIGURE 2. A plot of Θ ($z = \frac{1}{2}$) for an $m = 5$ fast mode at $\Omega = 500$, $\sigma = 7.0$ in a $\Gamma = 1$ cylinder, for boundary conditions A. For this mode $R_c^{(5)} = 35989.6$, $\omega_c^{(5)} = 26.884$.

of §3.2. The system is specified by three parameters: the dimensionless rotation rate Ω, the aspect ratio Γ, and the Prandtl number σ. In all the calculations we use Prandtl numbers in the range $6.7 \leqslant \sigma \leqslant 7.0$ appropriate to the experiments of Zhong *et al.* (1991) and Ecke *et al.* (1992). The experiment was carried out for aspect ratio $\Gamma = 1$; new cells of aspect ratio $\Gamma = 2.5$ and 5 have been built and results for these will therefore be forthcoming. In the following we focus on the dependence of $R_c^{(m)}$ and $\omega_c^{(m)}$ on both Ω and Γ for different values of the azimuthal wavenumber m.

The results for boundary conditions A, (14)–(15), are presented in figure 1. Figure 1(*a*) shows $R_c^{(m)}$ as a function of Ω for $\Gamma = 1$, $\sigma = 7.0$. Each curve is labelled by its m-value. Figure 1(*b*) shows the corresponding frequencies $\omega_c^{(m)}$. Note that the $m = 0$ state (concentric circular rolls) does not precess. This is because it does not break the $SO(2)$ symmetry of the system. For small rotation rates, $m = 1$ is the preferred mode (i.e. the one with the lowest critical Rayleigh number) in agreement with the non-rotating result (Marqués *et al.* 1992); with increasing Ω, the preferred value of m increases. Note that R_c, the critical Rayleigh number minimized over m, is typically significantly smaller than that predicted for an unbounded layer (Chandrasekhar 1961), and that for $m > 2$ the increase of $R_c^{(m)}$ with Ω is noticeably slower than that of $R_c^{(0)}$.

All of the modes represented in figure 1 are of the spiral type observed by Zhong *et al.* (1991) and Ecke *et al.* (1992). In figure 2 we show a plot of the contours of Θ at the midplane, $z = \frac{1}{2}$, for an $m = 5$ mode and typical parameter values of their experiments: $\Gamma = 1$, $\Omega = 500$, $\sigma = 7$. For these parameter values $R_c^{(5)} = 35989.6$ and $\omega_c^{(5)} = 26.884$. These modes are characterized by a small amplitude in the centre of the container and peak amplitude near the boundary and are, except for their precession, similar to the spoke-like pattern described by Buell & Catton (1983*b*). We refer to them as the *fast* modes, on account of their relatively large precession frequency $\omega_c^{(m)}$. Figure 3(*a*) shows $R_c^{(m)}$ for the fast modes as a function of Γ for $\Omega = 500$ and several different values of m. Figure 3(*b*) shows the corresponding frequencies $\omega_c^{(m)}$. Observe that the preferred mode number m slowly increases with Γ,

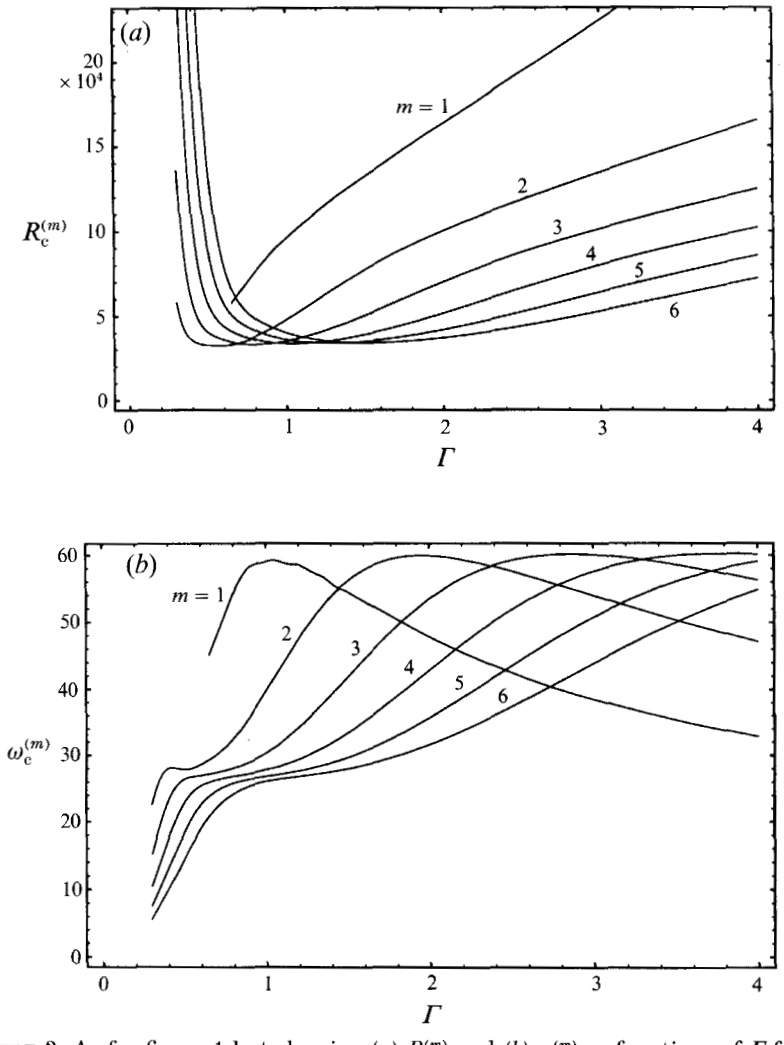

FIGURE 3. As for figure 1 but showing (*a*) $R_c^{(m)}$ and (*b*) $\omega_c^{(m)}$ as functions of Γ for $\Omega = 500$.

but that the difference between the critical Rayleigh numbers for the different m-values remains small, at least for modes with $m \geqslant 3$. Note also that the $R_c^{(m)}$ appear to increase rapidly with increasing Γ, as does the corresponding precession frequency, at least initially.

In addition to the fast modes described above, another type of precessing mode is present as well. These modes have a completely different character and the precession rate is typically two or three orders of magnitude slower than that of the fast modes. Consequently, we refer to them as the *slow* modes. In contrast to the fast modes the critical Rayleigh number (figure 4*a*) and the precession frequency (figure 4*b*) of these modes both decrease with increasing aspect ratio, albeit in an oscillatory manner. Moreover, with increasing aspect ratio a fast mode with a given mode number m is always superseded by the corresponding slow mode although there may be other fast modes with yet lower values of R_c. For the example illustrated in figure 5 the critical Rayleigh number for the slow $m = 1$ mode crosses that for the corresponding fast mode at $\Gamma = 1.01$; for larger values of Γ the slow mode has a lower

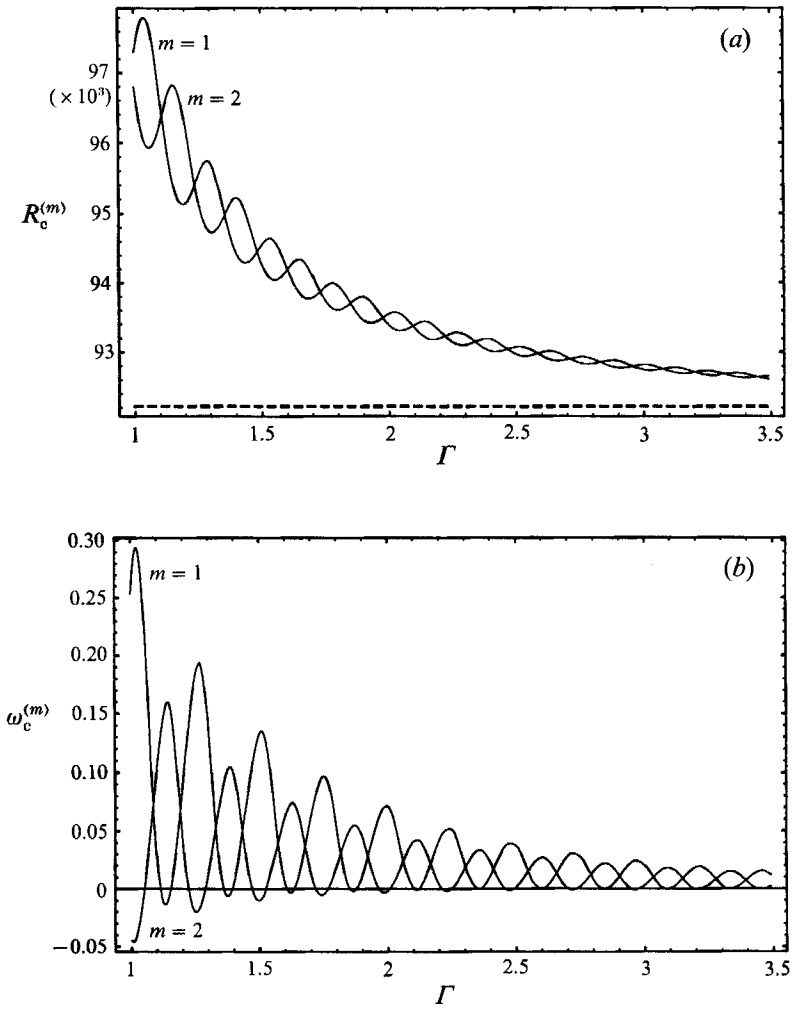

FIGURE 4. As for figure 3 but for the slow modes with $m = 1$ and $m = 2$. The value of R_c for an unbounded layer is indicated by a dashed line.

critical Rayleigh number (solid line) than the fast mode (dotted line). For $m = 2$ the corresponding critical aspect ratio is 1.84. From figures 4 and 5 it appears that it is the slow modes that approach Chandrasekhar's linear stability result as $\Gamma \to \infty$, i.e. $R_c \to R_\infty$, $\omega_c \to 0$, expected for a $\sigma = 7.0$ fluid in an unbounded layer. This conclusion is supported by the structure of the slow modes. Figures 6 and 7 compare the fast and slow modes with $m = 2$ and $m = 5$ for $\Omega = 500$, $\sigma = 7.0$ at the critical aspect ratios at which the slow modes supersede the corresponding fast modes, i.e. at $\Gamma = 1.84$ for $m = 2$ and $\Gamma = 4.39$ for $m = 5$. The fast modes are in effect wall-driven modes, of negligible amplitude near the centre of the cylinder, and large amplitude near the sidewall. In contrast, the slow modes are body modes, with large amplitude in the inner part of the cylinder away from the sidewall, and low amplitude near it. As a consequence, if one measures the degree of asymmetry of the fast and slow modes, this asymmetry is more pronounced in the fast modes and less in the slow modes (see figure 8). Since the precession rate depends on the asymmetry of the modes, one expects the body modes to indeed precess more slowly than the wall modes, as

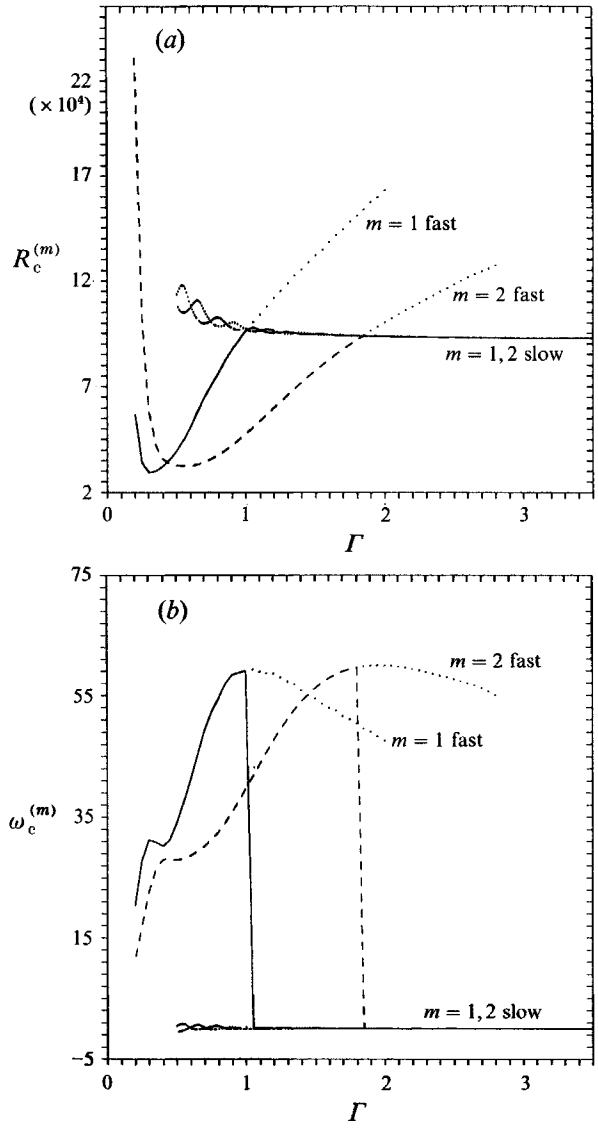

FIGURE 5. The transition from the fast modes with $m = 1$ and $m = 2$ for $\Omega = 500$, $\sigma = 7.0$ to the corresponding slow modes with increasing aspect ratio, for boundary conditions A. (*a*) The critical Rayleigh numbers, and (*b*) the corresponding precession frequencies.

observed. Note, finally, that typically $\omega_c^{(m)} > 0$, i.e. the precession frequency is counter to the direction of rotation, although for the slow modes it is possible in certain cases to get precession in the rotation direction. Another way to look at the transition between the fast and slow modes is to consider a fixed-aspect-ratio cylinder and increase Ω. For example, for $\Gamma = 1$ and boundary conditions A one finds several transitions between the fast and slow $m = 1$ modes as Ω increases (figure 9). For $m > 1$ the fast mode always has a lower critical Rayleigh number. The delicate behaviour of the $m = 1$ modes is present in this case because the $m = 1$ fast and slow modes cross at $\Gamma = 1.01$ when $\Omega = 500$, $\sigma = 6.7$. Note that when a slow mode in a small to moderate aspect ratio cylinder (e.g. $\Gamma = 1$) is preferred over a fast mode of the same mode number, there is generally a fast mode of a different wavenumber that

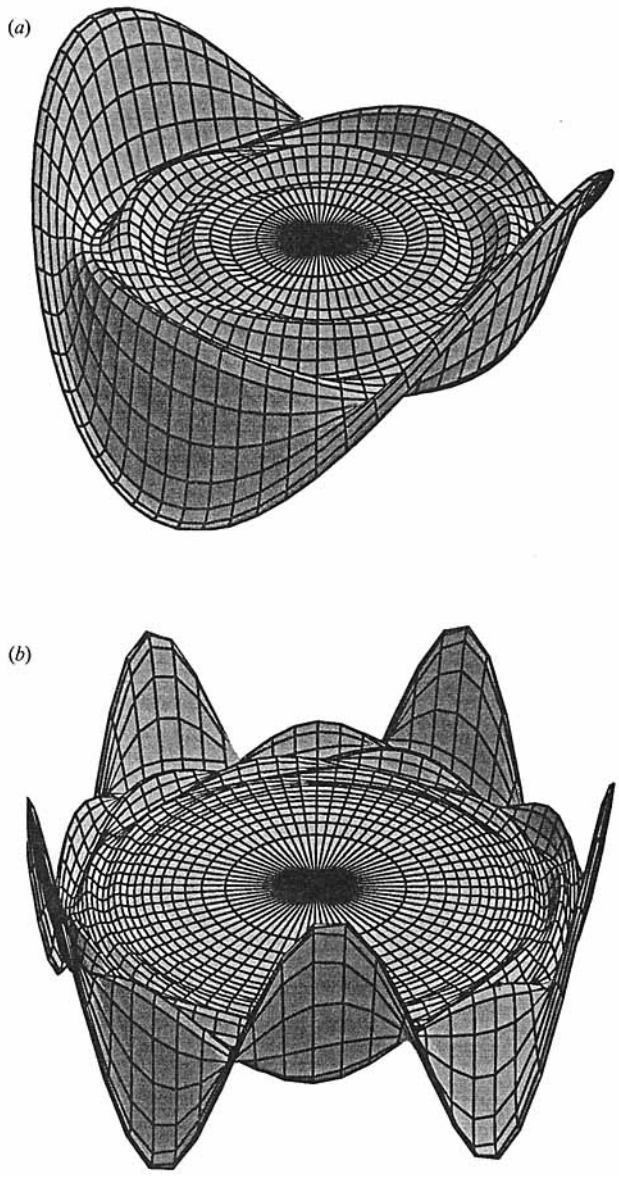

FIGURE 6. As for figure 2 but for (*a*) an $m = 2$ mode with $\Gamma = 1.84$, and (*b*) an $m = 5$ mode with $\Gamma = 4.39$. For these modes $R_c^{(2)} = 93682$, $\omega_c^{(2)} = 59.8$, and $R_c^{(5)} = 92486$, $\omega_c^{(5)} = 60.1$.

is already unstable. This is no longer so for larger aspect ratios, where a slow mode can be the first to set in (see below).

For comparison we include in figure 10 curves of $R_c^{(m)}$ as a function of the rotation rate for $\Gamma = 1$, $\sigma = 6.7$ and a conducting sidewall and stress-free boundaries at top and bottom. In this case the mode $m = 1$ continues to be preferred for small rotation rates, but $m = 0$ is selected for $9 < \Omega < 22$, followed by $m = 2$ and higher values of m as Ω increases. These modes are all fast. The critical Rayleigh numbers are somewhat higher than the corresponding ones for an insulating sidewall for all rotation rates examined. This effect of the sidewall conductivity had already been observed for the non-rotating cylinder with no-slip boundary conditions by Buell &

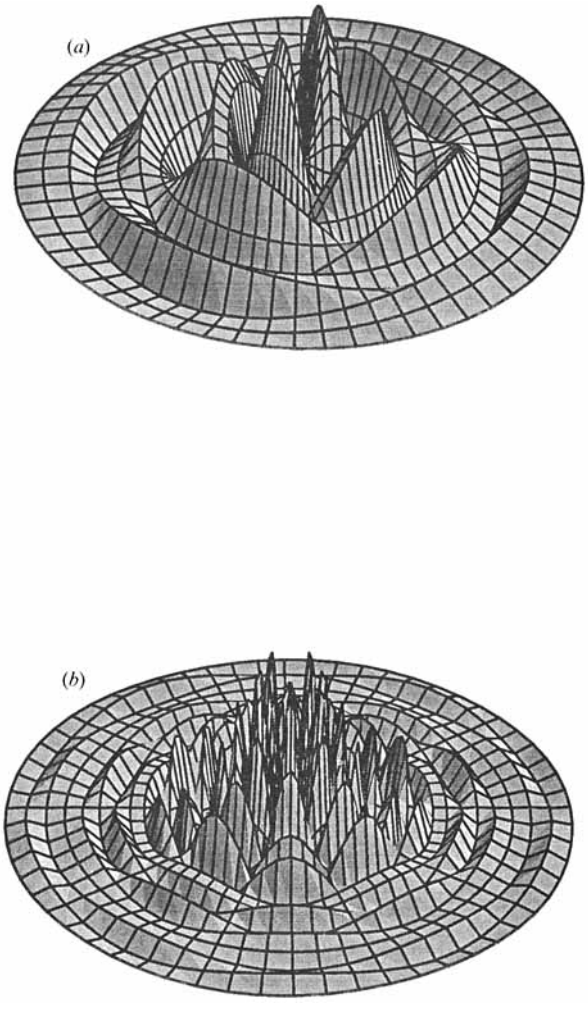

FIGURE 7. As for figure 6 but for slow modes. (*a*) $m = 2$ mode with $\Gamma = 1.84$ and (*b*) $m = 5$ mode with $\Gamma = 4.39$. For these modes $R_c^{(2)} = 93682$, $\omega_c^{(2)} = 0.0457$, and $R_c^{(5)} = 92486$, $\omega_c^{(5)} = 0.00344$.

Catton (1983*a*). More relevant to the experiments is the case of an insulating sidewall and rigid (no-slip) boundaries at the top and bottom. In figure 11 (*a*, *b*) we show a comparison between the marginal stability boundaries R_c for boundary conditions A and B together with the corresponding precession frequencies ω_c as a function of Ω. Data from the experiment of Zhong *et al.* (1991) are also included. For large rotation rates ($\Omega \geqslant 2 \times 10^2$), there is very little difference between the marginal stability curve for stress-free and no-slip boundaries; a similar result for an unbounded layer (and hence for non-precessing patterns) is well-known (Niiler & Bisshopp 1965). However, an analogous result for rapidly rotating cylinders by Homsy & Hudson (1971) is suspect since the possibility of precession was not recognized. In contrast, for small Ω the critical Rayleigh numbers are substantially larger for no-slip boundary conditions (cf. Marqués *et al.* 1992), while the precession velocities are lower. An important qualitative difference between the results for boundary conditions A and B is that it is the mode $m = 0$ that is now preferred in $\Gamma = 1$ cylinders. As already explained, this mode does not precess. At $\Omega = 28$ this mode is superseded by an

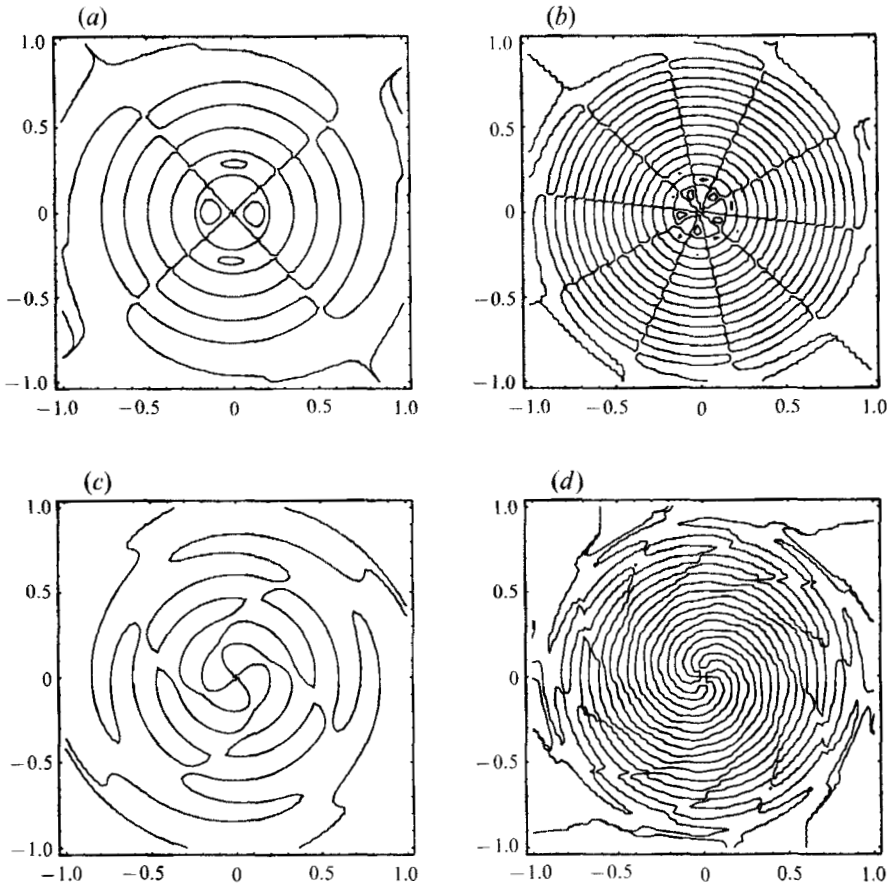

FIGURE 8. Contour plots of $\Theta(z = \frac{1}{2}) = 0$ for the modes depicted in figures 6 and 7: (*a*) $m = 2$ slow mode, (*b*) $m = 5$ slow mode, (*c*) $m = 2$ fast mode, and (*d*) $m = 5$ fast mode. The axes are scaled in units of r/Γ.

$m = 2$ fast mode; this mode does precess, and its precession rate is once again counter to the rotation, increasing monotonically with Ω from its value at $\Omega = 28$ (see figure 11*b*).

We conclude this section by presenting the corresponding results for $\Gamma = 2.5$ with both sets of boundary conditions and $\sigma = 6.8$. Figure 12(*a*) shows R_c as a function of Ω, compared with the experimental values obtained by R. Ecke and F. Zhong (private communication). Figure 12(*b*) shows the corresponding ω_c, together with the preferred values of m. Figures 12(*c*) and 12(*d*) show enlargements of figure 12(*b*) for boundary conditions A and B, respectively, and small rotation rates Ω. For boundary conditions A the mode that first appears for $0 < \Omega \leqslant 4.6$ is an $m = 1$ slow mode. With increasing Ω the selected azimuthal wavenumber jumps successively to $m = 2$, $m = 0$, and then $m = 1$. All these modes are slow modes (i.e. body modes) and in some intervals of Ω (e.g. $4.6 < \Omega \leqslant 5.4$) they precess in the direction of rotation. For $11.8 < \Omega < 18.4$ the first unstable mode is an $m = 6$ fast mode; for larger Ω the first unstable modes are all fast modes, with ever-increasing azimuthal wavenumbers. In contrast, for boundary conditions B one finds that for $\Omega < 9$ it is the $m = 0$ mode that is selected; for $9 \leqslant \Omega \leqslant 25$ the preferred mode is an $m = 1$ slow mode while the $m = 2$ slow mode is preferred for $25 < \Omega \leqslant 38.5$. At $\Omega \approx 38.5$ the preferred mode jumps to an $m = 8$ fast mode and remains a fast mode thereafter, with the mode

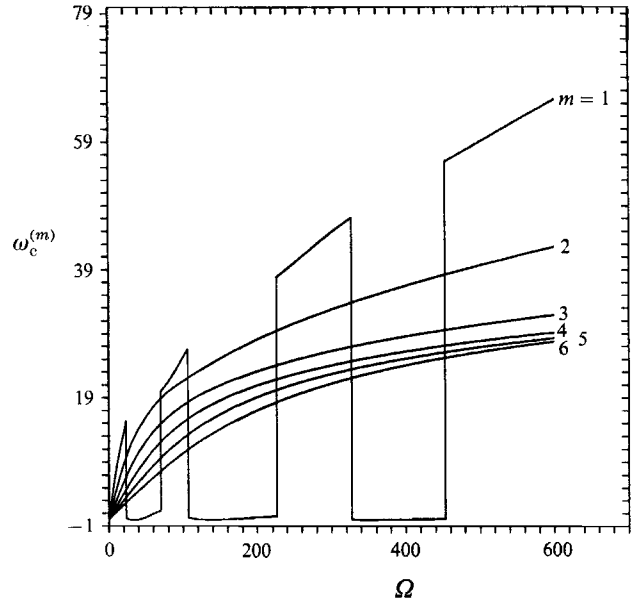

FIGURE 9. The competition between the fast and slow modes for different values of m as a function of Ω for fixed $\Gamma = 1$, $\sigma = 6.7$, and boundary conditions A. Note that for $m \geqslant 2$ the fast modes always have lower critical Rayleigh number than the corresponding slow modes; for $m = 1$ it is either the fast or the slow mode that has a lower critical Rayleigh number, depending on Ω.

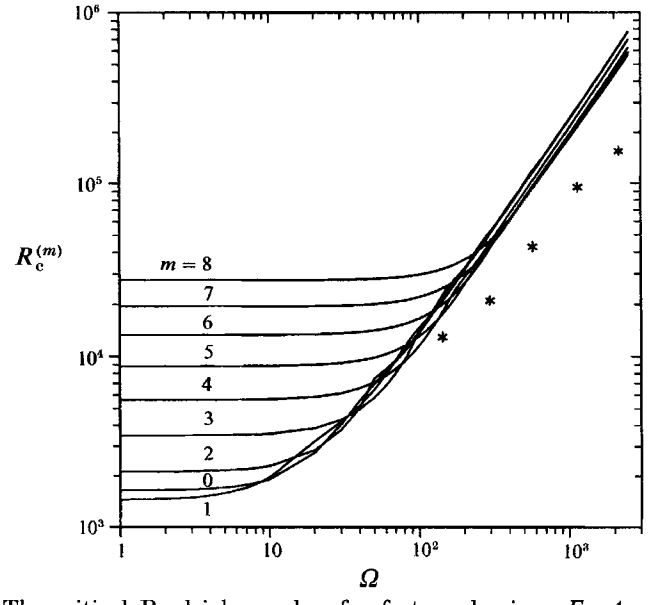

FIGURE 10. The critical Rayleigh number for fast modes in a $\Gamma = 1$ cylinder with boundary conditions A, but thermally conducting sidewall, and $\sigma = 6.7$. The points indicate the data from Zhong *et al.* (1991). The slow modes always have a higher critical Rayleigh number than the corresponding fast modes.

number gradually increasing with Ω (see figure 12*b*). The identification of the modes as slow and fast modes in the above discussion is based not only on the precession frequencies but also on their spatial structure.

Note, finally, that for both $\Gamma = 1$ and 2.5 the mode that is selected in case B for

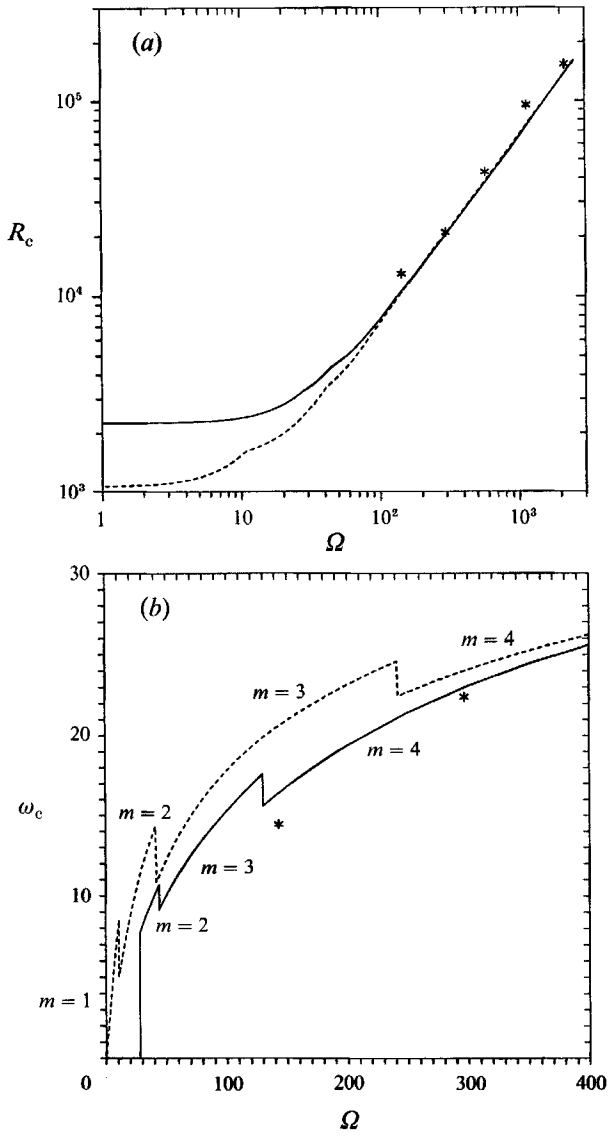

FIGURE 11. A comparison between (*a*) the critical Rayleigh numbers R_c minimized over m and (*b*) the corresponding precession frequencies for boundary conditions A (- - - -) and B (——) as a function of Ω when $\Gamma = 1$, $\sigma = 6.7$. The selected mode numbers are indicated in (*b*). The results for the rigid boundary conditions, B, agree well with the experimental data of Zhong *et al.* (1991), shown as stars.

small Ω is $m = 0$. Consequently the suggestion by Ecke *et al.* (1992) that for small Ω one should find $\omega_c = \delta\Omega + O(\Omega^3)$ only applies to boundary conditions A. For $\Gamma = 1$, $\sigma = 6.7$ one then finds that the preferred mode has $m = 1$, with $\delta = 0.127$. This value is close to that deduced for boundary conditions B by Ecke *et al.* i.e. $\delta = 0.1 \pm 0.02$, although it must be recognized that the latter is an approximation to the jagged curve shown in figure 11 (*b*), and is not valid as $\Omega \to 0$.

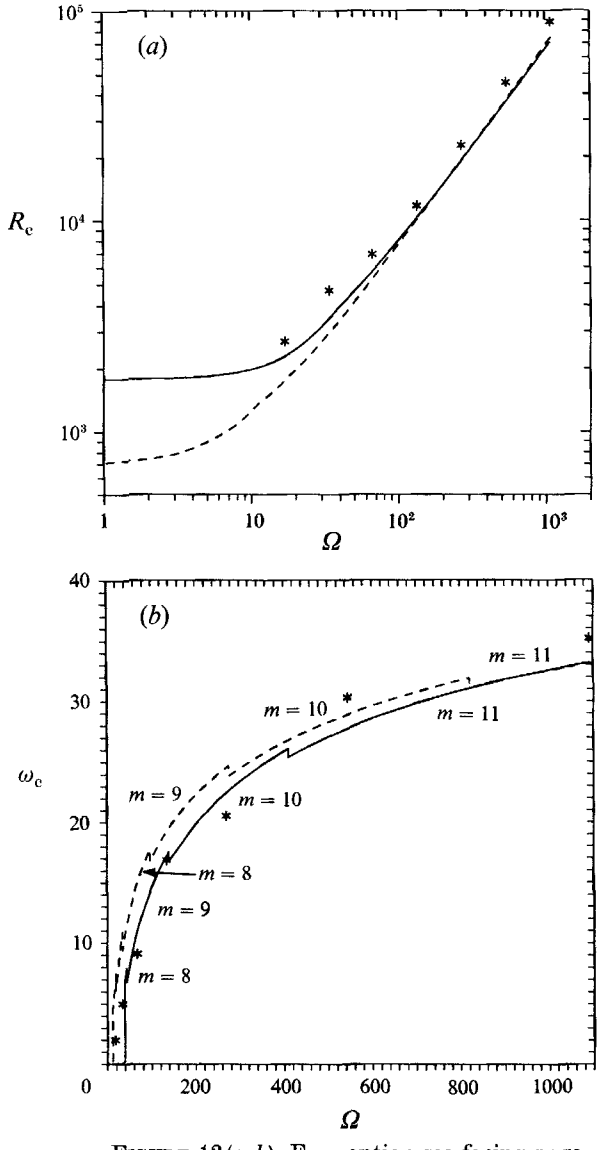

FIGURE 12(*a*, *b*). For caption see facing page.

5. Discussion

In this paper we have considered the linear stability problem for the onset of convection in a uniformly rotating right circular cylinder heated from below. We found, in contrast to earlier work of Buell & Catton (1983*b*), but in agreement with a generic argument based on the absence of reflection symmetry in vertical planes, that the convective instability is a Hopf bifurcation whenever the azimuthal wavenumber of the mode is non-zero. Such an instability therefore gives rise to a type of precessing pattern called a rotating wave. We found there are two types of such precessing patterns, distinguished by both their structure and their precession rate. We have called these the fast and the slow modes. For small to moderate aspect ratios the conduction state always loses stability to a fast mode as the Rayleigh number increases; these take the form of m-armed spirals much like those observed

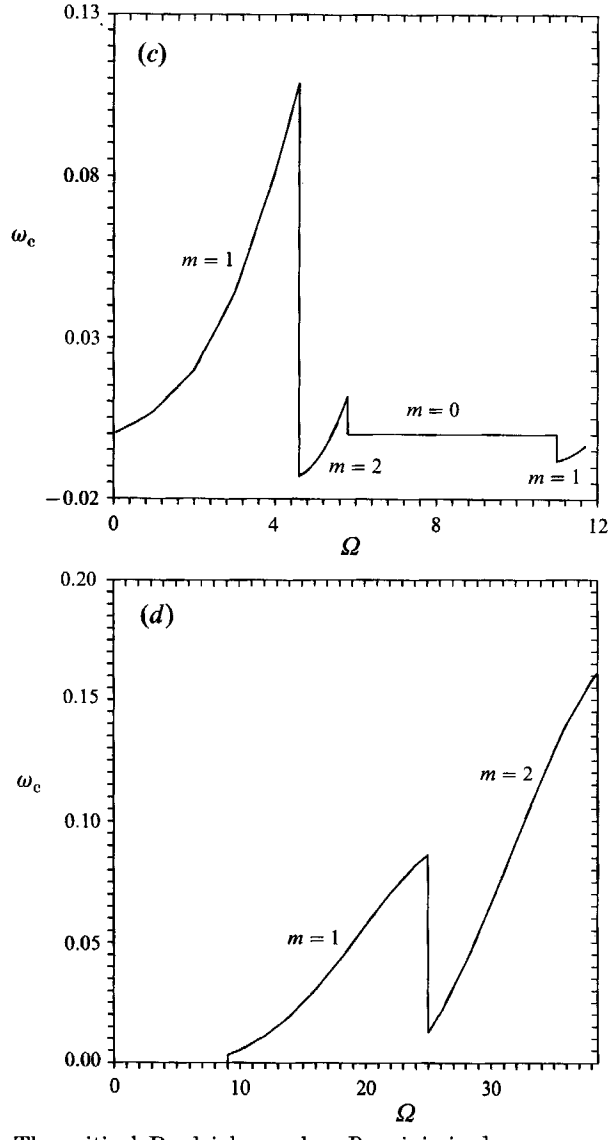

FIGURE 12. (*a*) The critical Rayleigh number R_c minimized over m and (*b*) the corresponding precession frequency as a function of Ω in a $\Gamma = 2.5$ cylinder with $\sigma = 6.8$ and boundary conditions A (----) and B (——). The data points show unpublished data kindly provided by R. Ecke and F. Zhong. (*c*, *d*) Enlargements of (*b*) for small Ω: (*c*) boundary conditions A; (*d*) boundary conditions B.

by Zhong *et al.* (1991), Ecke *et al.* (1992). The amplitude of these modes peaks near the sidewall and they may be called wall modes. For larger aspect ratios the first mode to go unstable may be a slow mode provided the rotation rate is sufficiently slow. In contrast to the fast modes, the amplitude of the slow modes is low near the sidewall and peaks in the inner part of the cylinder. Such modes may therefore be called body modes. The slow modes play an important role in understanding both the large-aspect-ratio limit of the present calculation, and the experiments. As Γ increases, the precession rate of the slow modes tends toward zero, while the critical Rayleigh number for their onset approaches the Chandrasekhar result. These results

enable us for the first time to establish the connection between the solution of the linear stability problem in a rotating unbounded plane layer and in a rotating cylinder of large but finite aspect ratio. In particular, our analysis enables us to reconcile Chandrasekhar's result that unless the Prandtl number is small the instability is a steady-state one and the symmetry argument showing that in a cylindrical container the instability should always be a Hopf bifurcation, regardless of the value of the Prandtl number. The only exception to the argument is provided by a pattern of concentric rolls, which does not break the circular symmetry and does not precess. In nearly all cases the precession was found to be counter to the rotation rate, although with boundary conditions A it is possible to find parameter values when $\Gamma = 2.5$ such that the first mode to set in precesses in the direction of rotation. We have found no examples of this behaviour with boundary conditions B.

Although a slow mode always supersedes a fast mode with the same mode number as the aspect ratio increases, when this happens in moderate-aspect-ratio ($\Gamma \lesssim O(1)$) cylinders there is always a fast mode with a different mode number that is already slightly unstable. However, even in this case the slow mode may manifest itself. Indeed, in the experiments the fast mode appears to be present for only slightly supercritical Rayleigh numbers; with increasing R the observed pattern evolves into one that looks like the slow mode, i.e. the central region of the cylinder fills in relatively abruptly once the Rayleigh number is sufficiently large. We interpret this transition as a secondary bifurcation from a branch of pure fast modes with increasing Rayleigh number. Such a bifurcation gives rise to a mixed mode, consisting of a nonlinear superposition of the wall and body modes, with the body modes dominating with increasing R, in qualitative agreement with observations (R. Ecke, private communication). Note that such a mixed mode will in fact be quasi-periodic, although the slow frequency may be too small to be detected experimentally. In smaller-aspect-ratio cylinders a similar mechanism is responsible for the observed transitions between fast modes with different azimuthal wavenumbers (cf. Zhong *et al.* 1991), while in larger-aspect-ratio cylinders it may be the slow mode that is the primary mode of instability, at least for sufficiently small rotation rates. In all cases examined we have found that with increasing rotation rate the primary mode changes from a slow mode with a low azimuthal wavenumber to a fast mode with a significantly larger azimuthal wavenumber. We do not know whether there is a critical aspect ratio Γ_c such that for $\Gamma > \Gamma_c$ the first unstable mode is a slow mode for all rotation rates. This question should be answerable by examining the $\Gamma \to \infty$ or equivalently the $k \to \infty$ limit of the dispersion relation (27), (28).

To facilitate comparison with the experiments, we have included in figures 10 and 11 the measured values of R_c and ω_c from the Zhong *et al.* (1991) experiment. This experiment was carried out for water with a Prandtl number of 6.7 in a cylinder of aspect ratio $\Gamma = 1$, with a thermally insulating Plexiglas sidewall. The sapphire top and copper bottom are both excellent thermal conductors. Consequently the experiment is best modelled by our boundary conditions B (equations (16)–(17)), and indeed we observe in general a very good agreement between the theoretical linear stability results for these boundary conditions. The agreement in R_c is better, with the experimental points falling (with one exception) slightly above the theoretical ones. The precession frequencies fall above the predicted values by about 8% for larger rotation rates ($\Omega \geqslant 700$), but below them (by about 13%) for smaller rotation rates ($\Omega \leqslant 500$). With a conducting sidewall the critical Rayleigh number is shifted towards larger values and the agreement with the data is worse (see figure 10). This is also the case for stress-free boundaries which yield critical Rayleigh numbers that

are, for slow rotation rates, substantially lower than those for no-slip boundary conditions.

It is also important to compare the predicted values of the azimuthal mode number m with the measured ones. With boundary conditions B and $\sigma = 6.7$ we find that $m = 3$ for $44 < \Omega < 130$, $m = 4$ for $130 < \Omega < 1500$ and $m = 5$ for $\Omega > 1500$ (see figure 11). In contrast Zhong *et al.* (1991) find that at $\Omega = 142$ the observed value of m is 3, while $m = 4$ is observed in the range $290 < \Omega < 1100$, and $m = 5$ is observed at $\Omega = 2145$ and $\Omega = 4274$. These results are not far from the predicted ones, but the origin of the discrepancy remains unclear. It is likely to be related to the proximity of the critical Rayleigh numbers of the various m-values (see e.g. figure 3*a*). Similarly, we have included in figure 12 unpublished data provided by R. Ecke and F. Zhong from their ongoing experiments with a $\Gamma = 2.5$ cylinder. As for $\Gamma = 1$, the quantitative agreement is excellent.

The results presented in this paper were obtained by two methods, of which the first is in principle exact for boundary conditions A, but does not generalize to other boundary conditions. The second method is spectral and uses a formulation of the problem in terms of velocity potentials. This method can be used not only for a variety of boundary conditions, but the formulation is in addition designed to enable us to tackle the nonlinear problem. The linear stability results presented here are a first step in this direction.

We are indebted to R. Ecke and F. Zhong for providing us with detailed data from their experiments. E.K. would like to thank J. M. Massaguer for his invitation to Barcelona, where this collaboration began. The work at Berkeley was supported by an INCOR grant from Los Alamos National Laboratory; that in Barcelona was supported by a DGYCIT grant PB91-0595.

REFERENCES

BUELL, J. C. & CATTON, I. 1983*a* The effect of wall conduction on the stability of fluid in a right circular cylinder heated from below. *Trans. ASME* C: *J. Heat Transfer* **105**, 255–260.

BUELL, J. C. & CATTON, I. 1983*b* Effect of rotation on the stability of a bounded cylindrical layer of fluid heated from below. *Phys. Fluids* **26**, 892–896.

BUSSE, F. H. 1978 Non-linear properties of thermal convection. *Rep. Prog. Phys.* **41**, 1929–1967.

CATTON, I. & EDWARDS, D. K. 1970 Initiation of thermal convection in finite right circular cylinders. *AIChE J.* **16**, 594–601.

CHANDRASEKHAR, S. 1961 *Hydrodynamic and Hydromagnetic Stability.* Dover.

CHOSSAT, P. 1982 Interactions entre bifurcations par brisure partielle de symétrie sphérique. *Ann. Sci. Éc. Norm. Sup.* **4** (15), 117–145.

ECKE, R. E., ZHONG, F. & KNOBLOCH, E. 1992 Hopf bifurcation with broken reflection symmetry in rotating Rayleigh–Bénard convection. *Europhys. Lett.* **19**, 177–182.

GOLDSTEIN, H. F. & KNOBLOCH, E. 1991 Linear stability of rotating Rayleigh–Bénard convection in a finite cylinder. *Bull. Am. Phys. Soc.* **36**, 2649–2650.

HOMSY, G. M. & HUDSON, J. L. 1971 The asymptotic stability of a bounded rotating fluid heated from below: the conductive basic state. *J. Fluid Mech.* **45**, 353–373.

JONES, C. A. & MOORE, D. R. 1979 The stability of axisymmetric convection. *Geophys. Astrophys. Fluid Dyn.* **11**, 245–270.

JOSEPH, D. D. 1971 Stability of convection in containers of arbitrary shape. *J. Fluid Mech.* **47**, 257–282.

KÜPPERS, G. & LORTZ, D. 1969 Transition from laminar convection to thermal turbulence in a rotating fluid layer. *J. Fluid Mech.* **35**, 609–620.

MARQUÉS, F. 1990 On boundary conditions for velocity potentials in confined flows: Application to Couette flow. *Phys. Fluids* A **2**, 729–737.

MARQUÉS, F., MERCADER, I., NET, M. & MASSAGUER, J. M. 1992 Thermal convection in vertical cylinders. I: A method based on potentials of velocity. *Comput. Meth. Appl. Mech. Engng* (submitted).

MERCADER, I., NET, M. & FALQUES, A. 1991 Spectral methods for high order equations. *Comput. Meth. Appl. Mech. Engng* **91**, 1245–1251.

NIILER, P. P. & BISSHOPP, F. E. 1965 On the influence of Coriolis force on the onset of convection. *J. Fluid Mech.* **22**, 753–761.

RAND, D. 1982 Dynamics and symmetry. Predictions for modulated waves in rotating fluids. *Arch. Rat. Mech. Anal.* **79**, 1–37.

SABRY, M. N. 1984 Sur une nouvelle méthode intégrale et son application aux écoulements de fluides visqueux avec ou sans transfert de chaleurs. Ph.D. thesis, Institut National Polytechnique de Grenoble.

SCHLÜTER, A., LORTZ, D. & BUSSE, F. H. 1965 On the stability of steady finite amplitude convection. *J. Fluid Mech.* **23**, 129–144.

ZHONG, F., ECKE, R. E. & STEINBERG, V. 1991 Asymmetric modes and the transition to vortex structures in rotating Rayleigh–Bénard convection. *Phys. Rev. Lett.* **67**, 2473–2476.